

Simulation Study on the Effect of HIFU Irradiation Frequency and Duty Cycle Combination Parameter Optimization on Thermal Lesion of Biological Tissue

Hu Dong (PhD)^{1*}, Gang Liu (PhD)², Gaofeng Peng (MD)¹

ABSTRACT

Background: High-Intensity Focused Ultrasound (HIFU) represents a non-invasive treatment approach that utilizes non-ionizing radiation. This technique has found clinical utility in managing both benign and malignant solid tumors.

Objective: This study aimed to investigate the variations in HIFU frequency and duty cycle influence thermal lesion formation in tissue to identify the optimal parameter combination for HIFU therapy in multi-layered tissues.

Material and Methods: In this theoretical framework, a model of HIFU application to multi-layer biological tissues was created. Four unique HIFU parameter sets, defined by combining high or low frequency with high or low duty cycle, were comprehensively examined. The study analyzed how these settings influenced temperature distributions and lesion area in the layered tissue to ascertain the ideal combination of frequency and duty cycle parameters.

Results: Simulation results revealed that the former parameter set (high frequency, low duty cycle) was optimal for treating smaller, superficial tumours, whereas the latter combination (low frequency, high duty cycle) proved effective for deeper-seated lesions. Regarding thermal dose metrics, the high-energy setting (high frequency, high duty cycle) generated the most extensive lesion area and highest peak temperature, in contrast to the low-energy configuration (low frequency, low duty cycle), which produced the smallest coagulation zone and lowest focal temperature.

Conclusion: The study demonstrates that optimal HIFU therapeutic outcomes require frequency-duty cycle combinations tailored to tumour characteristics, with high-frequency/low-duty cycle for shallow small tumours and low-frequency/high-duty cycle for deep lesions, providing a framework for precision parameter selection in clinical applications.

Keyword

High-Intensity Focused Ultrasound; Lesion; Temperature; High-Frequency; Tumors; Radiation, Nonionizing; Treatment Outcome

Introduction

Medical ultrasound represents one of the most dynamic areas within modern ultrasound technology. Clinically, therapeutic applications primarily harness the phenomena of acoustic cavitation and thermal energy deposition induced by ultrasound waves,

¹School of Information Science and Engineering, Changsha Normal University, Changsha 410100, China

²School of Information Science and Engineering, Xinyu University, Xinyu, 338004, China

*Corresponding author:
Hu Dong
School of Information Science and Engineering, Changsha Normal University, Changsha 410100, China
E-mail: weijundong203@outlook.com

Received: 21 December 2024
Accepted: 24 June 2025

and the main applications are ultrasonic lithotripsy and High-Intensity Focused Ultrasound (HIFU) [1]. HIFU can cause the tissue at the lesion site to vibrate greatly, thereby achieving the effect of crushing stones [2]. The thermal effect of HIFU can make the focused area reach a high temperature rise in a short period of time; accordingly, the tumor tissue is thermally coagulated and necrotized to kill cancerous cells. At the same time, due to the good focusing effect, the acoustic energy does not cause thermal damage to tissues surrounding the focal zone, thereby achieving non-invasive treatment [3].

Some research has been conducted on the performance of HIFU irradiation frequency and duty cycle in vitro and in living tissue. Kung et al. employed pulsed HIFU (1 MHz, 5% duty cycle) combined with drugs to target the lesion area in F98 glioma-bearing rats. Compared with the control group using drug treatment alone, the tumor lesion area was doubled, proving the feasibility of HIFU combined with drugs to treat glioma [4]. Snipstad et al. used ultrasound with a frequency of 1 MHz without significant heating to irradiate the lesion area of glioma rats at intervals of 5 seconds for 60 minutes. The results showed that tumor blood flow was reduced by 36% compared with the control group (P -value <0.05), with a concurrent 75% inhibition of tumor volume growth (P -value <0.01), thereby demonstrating HIFU's efficacy in suppressing glioma progression [5]. Tian et al. used pulsed HIFU with a frequency of 1 MHz, a duty cycle of 5%, and a repetition rate of 1 Hz to induce the opening of the blood-brain barrier in rats with glioblastoma multiforme. Ultrasound irradiation resulted in a doubling of drug concentration within tumors compared to the non-treated control group. Consequently, tumor growth was significantly inhibited (65% reduction) and rat survival was prolonged by 18 days. These results demonstrated the feasibility of using HIFU to induce blood-brain barrier opening, a strategy that

enhances drug delivery in the context of brain tumor treatment [6]. Zhu et al. constructed an embolic stroke model in the brains of New Zealand white rabbits, using pulses with a transducer frequency of 1.5 MHz and a duty cycle of 0.1% for thrombolysis. Data revealed that the first animal cohort ($n=3$) employed an acoustic power of 275 W. None of the white rabbits were successfully thrombolized. Two of the four white rabbits in the second group using 415 W acoustic power were successfully thrombolized, and five of the seven white rabbits in the third group using 550 W acoustic power were successfully thrombolized, proving the cooperation of HIFU and demonstrating the feasibility of MRI imaging in the direction of thrombolysis [7]. Duclos et al. used HIFU with frequencies of 1.5 MHz and 2.5 MHz to irradiate six rats with brain tumors. MRI images and anatomy results showed that 2.5 MHz ultrasound did not cause burns on the skull. The focal temperature reached 68.3 ± 2.1 °C at 2.5 MHz, significantly higher than the 54.7 ± 3.5 °C observed at 1.5 MHz [8]. Quadri et al. developed a cerebral thrombosis model. Using a hemispherical transducer for transcranial MRgFUS set to 230 kHz center frequency and 10% duty cycle, they irradiated thrombi for 30 seconds, achieving 95% ablation [9].

It can be seen that as one of the important parameters of HIFU irradiation, duty cycle has been widely used in HIFU theory and practice research. Therefore, when selecting HIFU irradiation parameters, it is worth paying attention to the selection of reasonable duty cycle parameters. At the same time, HIFU irradiation frequency has an important influence on tissue thermal lesions. How to select a suitable irradiation frequency to cope with tumor tissue of different sizes, and depths is another issue worthy of in-depth consideration. In summary, how to choose a safe and effective combination of HIFU irradiation frequency and duty cycle needs further exploration to achieve the optimal HIFU irradiation lesion effect.

Material and Methods

Khokhlov-Zabolotskaya-Kuznetsov (KZK) equation

The sound field is theoretically analyzed using the KZK equation, and it takes into account the combined effects of diffraction, absorption, and nonlinearity in directional ultrasound. The nonlinear KZK equation has been widely studied. For thermoviscous media, the KZK equation can be expressed as follows [10]:

$$\frac{\partial p}{\partial z} = \frac{c_0}{2} \int_{-\infty}^t \nabla_{\perp}^2 p \cdot dt' + \frac{\delta}{2c_0^2} \frac{\partial^2 p}{\partial t'^2} + \frac{\beta}{\rho_0 c_0^3} p \frac{\partial p}{\partial t'} \quad (1)$$

where p represents the sound pressure in Cartesian coordinates, z is the coordinate along the direction of beam propagation, x and y are transverse coordinates, $t' = t - z/c_0$ is the delay's time variable, t is the time, c_0 is the sound speed, $\nabla_{\perp}^2 = \partial^2 / \partial x^2 + \partial^2 / \partial y^2$ is the transverse Laplace operator, ρ_0 is the density, and δ is the thermoviscous medium's acoustic diffusion coefficient. B/A is the medium's nonlinear characteristic, and the nonlinear coefficient is $\beta = 1 + B/2A$.

Through the implementation of suitable coordinate and variable transformations, equation (1) can be simplified as follows [11]:

$$\frac{\partial P}{\partial \sigma} = \frac{1}{4(1+\sigma)^2} \int_{-\infty}^{\tau} \left(\frac{b}{a} \frac{\partial^2 P}{\partial X^2} + \frac{a}{b} \frac{\partial^2 P}{\partial Y^2} \right) d\tau' + A \frac{\partial^2 P}{\partial \tau'^2} + \frac{N}{1+\sigma} \left(P \frac{\partial P}{\partial \tau'} \right) \quad (2)$$

where $\sigma = z/z_0$ is the dimensionless characteristic length of the axis with respect to $z_0 = \omega_0 ab / 2c_0$, ω_0 represents the angular frequency, a and b are the characteristic source sizes in the x and y directions. X and Y are the transverse coordinate transformations, $P = (1+\sigma)(p/p_0)$ is the modified sound source pressure amplitude, τ is the conversion delay time, $A = \alpha_0 z_0$ is the absorption parameter, α_0 is the attenuation coefficient, and $N = z_0 / z'$ is the nonlinear parameter z' is defined as $z' = \rho_0 c_0^3 / \beta \omega_0 p_0$. The following is the definition of the dimensionless KZK equation [12]:

$$\frac{\partial P}{\partial \sigma} = \frac{1}{4G} \int_{-\infty}^{\tau} \left(\frac{b}{a} \frac{\partial^2 P}{\partial X^2} + \frac{a}{b} \frac{\partial^2 P}{\partial Y^2} \right) d\tau' + A \frac{\partial^2 P}{\partial \tau'^2} + N \left(P \frac{\partial P}{\partial \tau'} \right) \quad (3)$$

where $\sigma = z/d$ is the dimensionless z axis

relative to the geometric focal length d . X and Y are dimensionless transverse coordinates about a and b as previously defined, P is the dimensionless pressure amplitude on the transducer surface with respect to the acoustic source p_0 , $G = z_0/d$ is the dimensionless focusing gain, $A = z_0 d$ is the absorption parameter, $N = d / z'$ is the nonlinear parameter. The transducer semi-aperture is defined as a_0 , r is the coordinate perpendicular to the axis, and $R' = r / a_0$.

One efficient numerical technique for resolving the KZK equation is the operator separation algorithm [12]. It is possible to suppose that nonlinear, diffraction, and absorption effects are independent of one another in sufficiently tiny steps. It is possible to rewrite the KZK equation using the operator separation approach as follows [13]:

$$\frac{\partial P}{\partial \sigma} = L_D(P) + L_N(P^2) + L_A(P) \quad (4)$$

where the following definitions apply to the operators for diffraction, absorption, and nonlinearity [14]:

$$L_D(P) = \frac{1}{4G} \int_{-\infty}^{\tau} \left(\frac{b}{a} \frac{\partial^2 P}{\partial X^2} + \frac{a}{b} \frac{\partial^2 P}{\partial Y^2} \right) d\tau' \quad (5)$$

$$L_A(P) = A \frac{\partial^2 P}{\partial \tau'^2} \quad (6)$$

$$L_N(P) = N \left(P \frac{\partial P}{\partial \tau'} \right) \quad (7)$$

Here, the Finite Difference Time Domain (FDTD) approach is used to solve the KZK equation numerically [15]. The near-field diffraction is solved using the Implicit Backward Finite Difference (IBFD) technique, while the far-field diffraction is solved using the Crank-Nicolson Finite Difference (CNFD) approach. To increase the time domain calculation's efficiency, the five-point IBFD and CNFD algorithms are used for calculation [16,17]. For the diffraction equation (5), the deviation of the Laplace five-point IBFD is, as follows [18].

$$\left(\frac{b}{a} \frac{\partial^2 P}{\partial X^2} + \frac{a}{b} \frac{\partial^2 P}{\partial Y^2} \right) \rightarrow \frac{1}{(\Delta X)^2} \left(\frac{b}{a} P_{i,j+1,l}^{k+1} + \frac{a}{b} P_{i,j-1,l}^{k+1} - 2 \left(\frac{b}{a} + \frac{a}{b} \right) P_{i,j,l}^{k+1} + \frac{a}{b} P_{i,j,l-1}^{k+1} + \frac{b}{a} P_{i,j,l+1}^{k+1} \right) \quad (8)$$

The superscript k of p is the axial propagation

index of the sound beam, and the subscripts i, j , and l respectively represent the transverse direction indices.

Transverse direction indices X and Y are represented by the subscripts i, j , and l , respectively, whereas the superscript k of p indicates the sound beam's axial propagation index. In the above derivation, the simplified assumption of $\Delta X = \Delta Y$ is used, and the trapezoidal rule is used to find the integral.

For the diffraction equation (5), the deviation of Laplace five-point CNFD is as follows [18,19]:

$$\left(\frac{b}{a} \frac{\partial^2 P}{\partial X^2} + \frac{a}{b} \frac{\partial^2 P}{\partial Y^2}\right) \rightarrow \frac{1}{2(\Delta X)^2} \left[\frac{b}{a} (P_{i,j+1,l}^{k+1} + P_{i,j-1,l}^{k+1}) + \frac{a}{b} (P_{i,j,l+1}^{k+1} + P_{i,j,l-1}^{k+1}) \right] - \left(\frac{b}{a} + \frac{a}{b}\right) (P_{i,j,l}^{k+1} + P_{i,j,l}^k) + \frac{a}{b} (P_{i,j,j-1}^{k+1} + P_{i,j,j-1}^k) + \frac{b}{a} (P_{i,j-1,l}^{k+1} + P_{i,j-1,l}^k) \quad (9)$$

A new variable Q is declared as $Q_{i,j,l}^{k+1} = P_{i,j,l}^{k+1} + P_{i,j,l}^k$ in order to streamline the computation and cut down on calculation time; the truncation error of this approach is around $(\Delta\sigma)^2$. Therefore, the calculation accuracy of the CNFD algorithm in the radial direction is higher than that of the IBFD algorithm. In order to obtain the same accuracy, a larger step size can be considered in the CNFD algorithm.

The following results are obtained by applying the five-point CNFD to the diffraction term associated with equation (5):

$$1 \leq j \leq (j_{\max} - 1), 1 \leq l \leq (l_{\max} - 1):$$

$$\begin{aligned} & -\frac{R}{16} \frac{b}{a} Q_{i,j+1,l}^{k+1} - \frac{R}{16} \frac{a}{b} Q_{i,j-1,l}^{k+1} + \left(1 + \frac{R}{8} \left(\frac{b}{a} + \frac{a}{b}\right)\right) Q_{i,j,l}^{k+1} \\ & - \frac{R}{16} \frac{a}{b} Q_{i,j,l-1}^{k+1} - \frac{R}{16} \frac{b}{a} Q_{i,j,l+1}^{k+1} = \frac{R}{8} \frac{a}{b} \sum_{m=1}^{i-1} Q_{m,j+1,l}^{k+1} + \frac{R}{8} \frac{a}{b} \sum_{m=1}^{i-1} Q_{m,j,l+1}^{k+1} \quad (10) \\ & - \frac{R}{4} \left(\frac{a}{b} + \frac{b}{a}\right) \sum_{m=1}^{i-1} Q_{m,j,l}^{k+1} + \frac{R}{8} \frac{a}{b} \sum_{m=1}^{i-1} Q_{m,j,l-1}^{k+1} + \frac{R}{8} \frac{b}{a} \sum_{m=1}^{i-1} Q_{m,j-1,l}^{k+1} + 2P_{i,j,l}^k \end{aligned}$$

In the above equation, $R = \Delta\tau(\Delta\sigma)_k / G(\Delta X)^2$. In equation (10), all Q items on the left are unknown, whereas all Q and P items on the right are known, and the direct sparse algorithm can be used to solve the diffraction equation.

Substitute the result of the diffraction equation calculation into the absorption equation (6) is shown as the initial condition, and use the IBFD algorithm to discretize the partial derivative of equation (6):

$$\frac{\partial P}{\partial \sigma} = \frac{1}{\Delta\sigma} (P_{i+1,j}^n - P_{i,j}^n) \quad (11)$$

$$\frac{\partial P}{\partial \tau^2} = \frac{1}{(\Delta\tau)^2} (P_{i+1,j}^{n+1} - 2P_{i+1,j}^n + P_{i+1,j}^{n-1}) \quad (12)$$

Substitute equations (11) to (12) into equation (6):

$$n = 1: (1 + 2U)P_{i+1,j}^n - UP_{i+1,j}^{n+1} = P_{i,j}^n \quad (13)$$

$$2 \leq n \leq n_{\max} - 2: -UP_{i+1,j}^{n-1} + (1 + 2U)P_{i+1,j}^n - UP_{i+1,j}^{n+1} = P_{i,j}^n \quad (14)$$

$$n = n_{\max} - 1: -UP_{i+1,j}^{n-1} + (1 + 2U)P_{i+1,j}^n - UP_{i+1,j}^{n+1} = P_{i,j}^n \quad (15)$$

where $U = A\Delta\sigma / (\Delta\tau)^2$, and the absorption equation can be solved by the Thomas algorithm [20].

Bioheat Transfer Equation (BHTE)

To investigate how the acoustic field affects the temperature field, the BHTE was used to simulate the temperature field [21,22]:

$$\rho_0 C_t = K_t \nabla^2 T - W_b C_b (T - T_b) + Q_v \quad (16)$$

ρ_0 and C_t are the medium's density and specific heat, respectively, in formula (16). The blood perfusion cooling term is the second term on the right, with W_b , C_b , and T_b standing for the blood perfusion coefficient, specific heat, and temperature, respectively. The first term on the right is the heat conduction term, with K_t representing the heat conduction coefficient. The cumulative amount of heat that the medium absorbs when ultrasound travels through it is the third word on the right. The following is an expression for the total heat generated by the acoustic field [23,24]:

$$Q_v = 2\alpha_0 I \quad (17)$$

I is the transducer's sound intensity, and α_0 is the medium's attenuation coefficient. The FDTD method is used to solve the BHTE [15].

Equivalent heat dose

The comparable heating time at 43 °C is the same as the thermal dosage used to describe the thermal lesion outcomes. R=0.5 when $T \geq 43$ °C; R=0.25 when $T < 43$ °C. 240 minutes at 43 °C is usually used as the threshold for visible thermal lesion to biological media [25,26]:

$$TD_{43^{\circ}C} = \int_{t_0}^t R^{43-T(\tau)} d\tau \quad (18).$$

Model for simulation

Figure 1 illustrates the creation of a two-dimensional axisymmetric simulation model of biological tissue exposed to HIFU radiation. An in vitro tissue model, water, and an ultrasonic transducer make up the simulation region. To prevent reflection and diffraction from affecting the target area sound field, a precisely matched layer is added to the model border. The direction of the transducer radius is the r-axis, and the direction of ultrasonic propagation is the z-axis. This study disregards the impact of cavitation on the focal temperature and biological tissue lesion in order to streamline the problem analysis. A concave spherical ultrasonic transducer serves as the HIFU source. Two situations of the irradiation frequency are separated: geometric focal length $d=13.0$ cm, transducer inner radius $a'=1.0$ cm, outer radius $b'=2.2$ cm,

high-frequency $f_H=3.0$ MHz, and low-frequency $f_L=0.8$ MHz. The output power of the transducer is 200 W, with 50% and 10% duty cycles at high and low, respectively. Ten seconds are spent irradiating with HIFU, and fifteen seconds are spent cooling. Ultrasound travels 7 cm in water, and the thicknesses of the skin, fat, muscle, and liver are 0.2, 1.0, 2.0, and 3.8 cm, respectively. To simulate the temperature field and acoustic field, the dynamic acoustic-thermal coupling model is employed [27].

Simulation parameters

The temperature field and acoustic field time steps are 0.003 s and 3.27×10^{-9} s, respectively, and the nonlinear harmonic order is 128. The test was conducted on a ThinkStation with an Intel i9 and 16.0 GB RAM, and the operating system was Windows 11. Table 1 lists the key acoustic and thermodynamic parameters of each medium (water, skin, fat, muscle, and liver) involved in the simulation, including density (ρ_0), sound

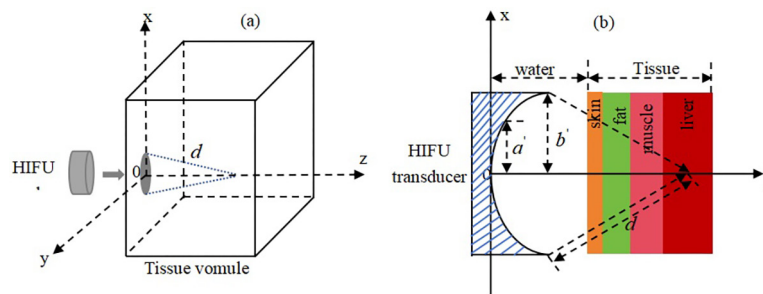


Figure 1: (a) Schematic diagram of the geometry of multi-layer biological tissue irradiated by High-Intensity Focused Ultrasound (HIFU) for simulation. (b) Schematic diagram of the ZX plane around $y=0$ (symmetric along the z axis)

Table 1: The medium's thermal and acoustic characteristics

Material	ρ_0 (kg/m ³)	c_0 (m/s)	α_0 (dB/m)	B/A	C_t (J/kg/K)	K_t (W/m/K)
Water	1000	1482	0.217	5.0	4180	0.60
Skin	1109	1400	115	7.0	3530	0.40
Fat	960	1476	36	10.3	2973	0.24
Muscle	1090	1550	200	4.5	3600	0.42
Liver	1036	1590	58	6.6	3604	0.53

speed (c_0), attenuation coefficient (α_0), non-linear characteristic (B/A), specific heat (C_p), and heat conduction coefficient (K_p). These parameters directly affect the propagation characteristics and energy deposition efficiency of ultrasound. For example, the high attenuation coefficients of skin and muscle (115 dB/m and 200 dB/m, respectively) indicate that they absorb ultrasound energy more strongly, which may lead to a more significant local temperature rise, while the low thermal conductivity of fat (0.24 W/m/K) may limit the diffusion of heat to surrounding tissues and aggravate local thermal lesions [28-32]. The KZK equation and the Biological Heat Conduction Equation (BHTE) can be numerically simulated using the parameters that were chosen based on experimental observations and literature verification, ensuring that the model can accurately predict the acoustic field distribution and thermal lesion effects of different tissues under HIFU irradiation.

Results

According to the tumor target area and size of HIFU treatment, the irradiation frequency and pulse parameters are adjusted to optimize the irradiation frequency and pulse combination parameters to achieve the best thermal lesion effect on the tumor.

Sound field simulation comparison

The sound intensity (Figure 2), positive pressure, and negative pressure (Figure 3) are generated in biological tissue by four

combinations of HIFU irradiation frequencies and duty cycles: low-frequency ultrasound and high duty cycle, low-frequency ultrasound and low duty cycle, high-frequency ultrasound and high duty cycle, and high-frequency ultrasound and low duty cycle (goal: precise therapy of superficial tissue or minor lesions).

By comparing the sound intensity generated by high-frequency ultrasound and low-frequency ultrasound inside biological tissue, it can be seen from Figure 2 that in the axial direction, the sound intensity generated by high-frequency ultrasound at the focal position of biological tissue is 2119 W/cm², while the sound intensity generated by low-frequency ultrasound at the focal position is 611.2 W/cm².

Comparing Figure 3 (a) and (c), the peak positive pressures generated by high-frequency and low-frequency focused ultrasound at the focal position of biological tissue are 23.8 MPa and 10.3 MPa, while from Figure 3 (b) and (d), it can be seen that the peak positive pressures generated by high-frequency and low-frequency focused ultrasound at the focal position of biological tissue are -3.7 MPa and -3.2 MPa. Obviously, high-frequency focused ultrasound is more likely to generate strong peak positive and negative pressures.

Temperature field simulation comparison

Based on the established acoustic-thermal coupling model, the simulated temperature distributions revealed distinct spatial patterns

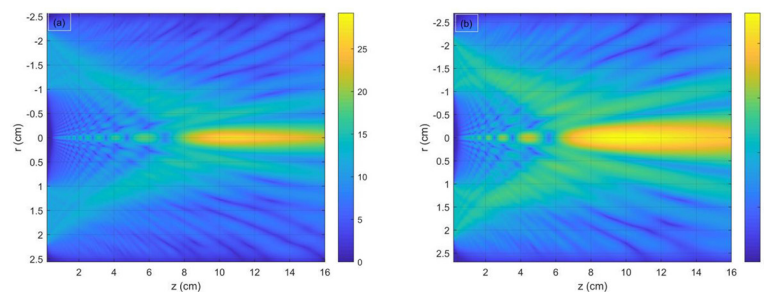


Figure 2: Comparison of sound intensity in biological tissue: (a) sound intensity generated by high-frequency ultrasound; (b) sound intensity generated by low-frequency ultrasound

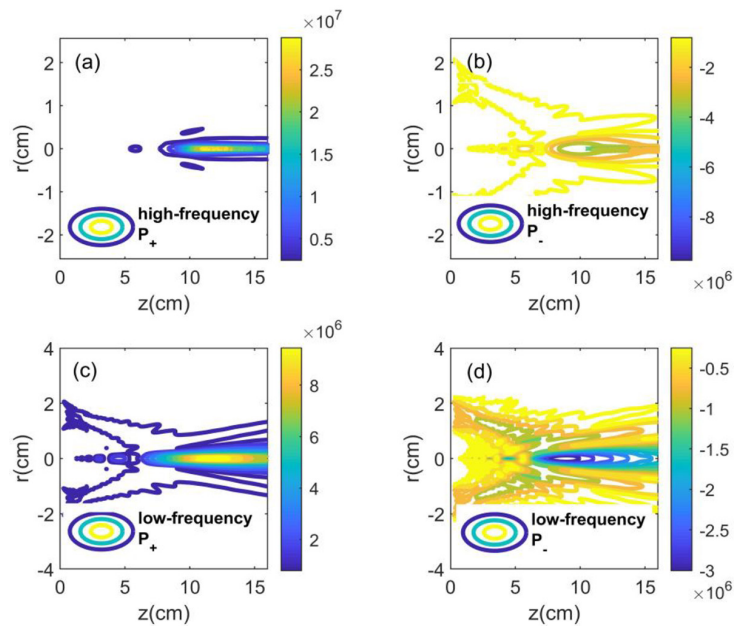


Figure 3: Comparison of positive and negative pressures in biological tissue: (a) positive pressure generated by high-frequency; (b) negative pressure generated by high-frequency; (c) positive pressure generated by low-frequency; (d) negative pressure generated by low-frequency

across the four parameter sets, with high-frequency exposures concentrating thermal energy near the focal zone, while low-frequency regimens promoted broader heat diffusion into deeper tissue layers.

Focus temperature comparison

The variations in biological tissue's focal temperature under four frequency and duty cycle combinations—high frequency and high duty cycle, high frequency and low duty cycle, low frequency and low duty cycle, and low frequency and high duty cycle—are depicted in Figure 4(a)-(d).

When the irradiation time is $t=10$ s, as illustrated in Figure 4, the focus temperature corresponding to the four distinct frequency and duty cycle combinations ((a) high-frequency and high duty cycle; (b) high-frequency and low duty cycle; (c) low-frequency and low duty cycle; and (d) low-frequency and high duty cycle) is the lowest at 62 °C, while the focus temperature corresponding to the high-frequency and high duty cycle combination is the highest at 569 °C. The focal

temperatures that correspond to the combinations of low frequency and high duty cycle and high frequency and low duty cycle are 93 °C and 298 °C, respectively.

Comparison of thermal lesion

The thermal lesion patterns exhibited pronounced variations across parameter combinations, where high-frequency/high-duty cycle configurations achieved maximal ablation extent while low-frequency/low-duty cycle minimized tissue damage, aligning with their respective targeting efficacy for deep and superficial tumors as visualized in Figure 5.

The thermal lesion area caused by HIFU irradiation of biological tissue was calculated using Photoshop software [33]. Figure 5 illustrates this for four distinct frequency and duty cycle combinations with the irradiation period $t=10$ s: (a) high frequency and high duty cycle; (b) high frequency and low duty cycle; (c) low frequency and low duty cycle; and (d) low frequency and high duty cycle. The thermal lesion area corresponding to the high-frequency and high duty cycle combination is the largest,

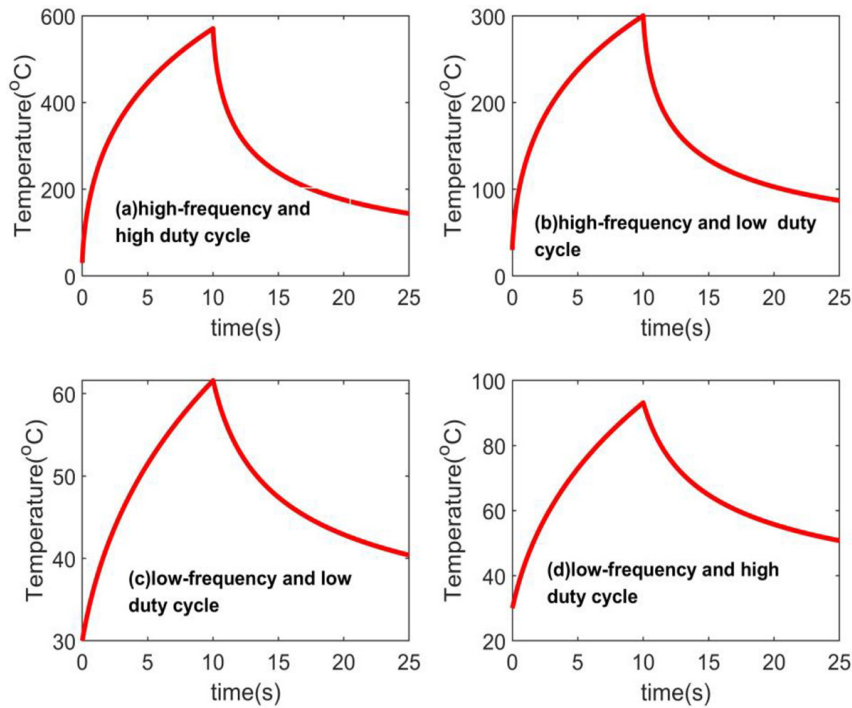


Figure 4: Focus temperature comparison: (a) high-frequency and high duty cycle; (b) high-frequency and low duty cycle; (c) low-frequency and low duty cycle; (d) low-frequency and high duty cycle

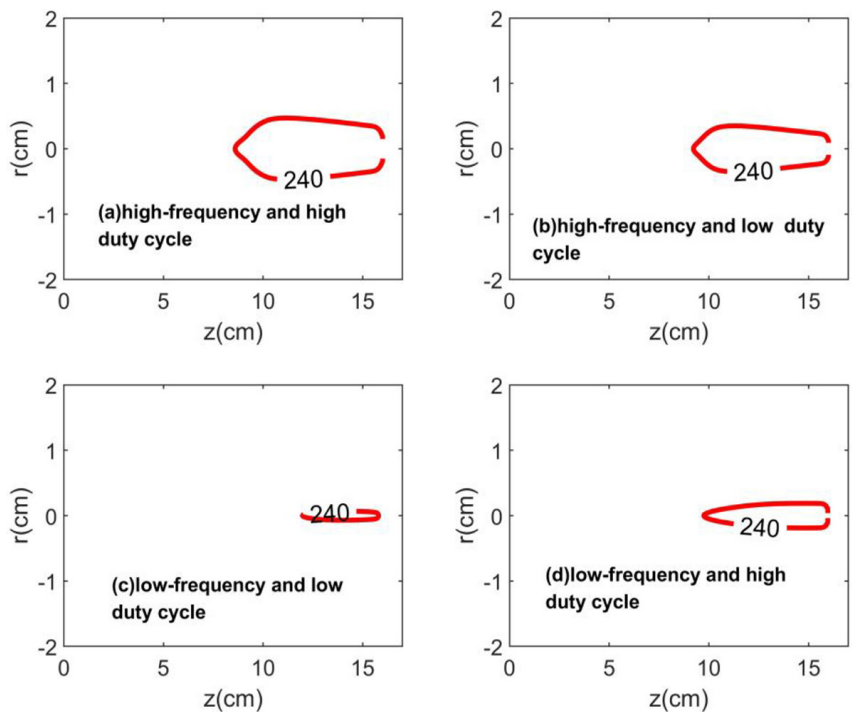


Figure 5: Comparison of thermal lesion: (a) high-frequency and high duty cycle; (b) high-frequency and low duty cycle; (c) low-frequency and low duty cycle; (d) low-frequency and high duty cycle

which is 6.49 cm^2 . However, at 0.60 cm^2 , the thermal lesion area associated with the combination of low frequency and low duty cycle is the smallest. The lesion areas that correspond to the combinations of low frequency and high duty cycle and high frequency and low duty cycle are 2.20 cm^2 and 4.52 cm^2 , respectively. Since high-frequency ultrasound has a shorter wavelength, the high-frequency and low duty cycle HIFU irradiation method is more suitable for the treatment of shallow tumors. Since low-frequency ultrasound has a longer wavelength and a deeper penetration depth, the low-frequency and high duty cycle HIFU irradiation method is more suitable for deep tumors.

Discussion

For the combination of high-frequency ultrasound and low duty cycle, high-frequency ultrasound usually has a higher frequency, a shorter wavelength, higher energy, and is easy to focus, but the penetration depth is relatively shallow [34,35]. Low duty cycle means that the ultrasound is “on” for a shorter time in the cycle and “off” for a longer time, resulting in lower energy output. Due to the high-frequency, when high-frequency ultrasound propagates in biological tissue, the energy is swiftly taken up and transformed into thermal energy, and the temperature at the focus will rise rapidly. However, due to the low duty cycle, the total energy output is reduced, so the temperature rise may be limited. The frequency of low-frequency ultrasound is lower, the wavelength is longer, the energy is lower, and the penetration depth is deeper when low-frequency ultrasound and high duty cycle are combined. A high duty cycle means that the ultrasound is “on” for a longer time in the cycle and “off” for a shorter time, resulting in higher energy output. Due to the long wavelength of low-frequency ultrasound, the rate at which energy is absorbed by biological tissue and converted into heat energy is slower [36], and the temperature rise at the focus is slower. However, a

high duty cycle increases energy output, thereby increasing the temperature at the focus. For the combination of low-frequency ultrasound and low duty cycle, low-frequency ultrasound has a deeper penetration depth but lower energy. A low duty cycle further reduces energy output. Due to low-frequency and low duty cycle, this combination produces relatively small temperature changes at the focus of biological tissue. High-frequency ultrasound is easier to focus due to its shorter wavelength and increased energy when combined with a high duty cycle. Energy output rises with a high duty cycle. The greatest temperature rise at the biological tissue’s focus is caused by the combination of high duty cycle and high frequency ultrasound. Fast-frequency ultrasonic energy is rapidly absorbed and transformed into thermal energy, and the fast duty cycle raises the overall energy output, which causes the temperature at the focus to rise quickly.

High-frequency ultrasound creates a powerful shock wave in tissue by propagating nonlinearly when combined with low duty cycle HIFU irradiation. The intensity of this shock wave is related to the peak negative pressure. The higher the peak negative pressure, the more obvious the nonlinear effect and the stronger the shock wave. A large number of microbubble clouds will be generated in the focal area during each pulse. The repeated expansion and collapse of these microbubbles will eventually cause the tissue to be crushed and form a clearly defined liquefied injury. Therefore, high-frequency ultrasound combined with a low duty cycle may produce a larger thermal lesion area, but due to the low duty cycle, the pulse duration is short and the energy deposition is less, which may limit the depth and range of the thermal lesion. For the low-frequency ultrasound and high duty cycle HIFU irradiation combination, a larger thermal lesion area will be generated because the high duty cycle means that the sound wave lasts longer, so that more energy is deposited in the tissue [37-39], resulting in

a greater thermal lesion. Studies have shown that as the duty cycle increases, the temperature rises faster inside the target area, and the necrotic volume increases with the increase in duty cycle. The combination of low-frequency ultrasound and low duty cycle HIFU irradiation will produce a smaller thermal lesion area, because the low duty cycle means that the duration of the sound wave is shorter and the energy deposition is less. This may lead to a smaller depth and range of thermal lesion, resulting in a smaller thermal lesion area. The biggest thermal lesion area will result from the combination of high duty cycle HIFU irradiation and high frequency ultrasound. High-frequency ultrasound itself produces strong shock waves due to nonlinear propagation, and a high duty cycle means more energy deposition. The combination of the two may lead to the largest thermal lesion area. In addition, high-frequency ultrasound under a high duty cycle can produce shock wave fronts in the focal area. After the tissue absorbs the shock wave, the temperature rises (>100 °C), and boiling bubbles are generated in the micron range, which expands into millimeter-sized bubbles [40,41]. After further interaction with the incoming shock wave, a very high negative pressure is generated, forming microbubble clusters, resulting in tissue fragmentation. In conclusion, the largest thermal lesion area and highest corresponding focal temperature are produced by combining high-frequency ultrasound with high duty cycle HIFU irradiation, while the smallest thermal lesion area and lowest corresponding focal temperature are produced by combining low-frequency ultrasound with low duty cycle.

Conclusion

This study explored the effects of HIFU irradiation frequency and pulse combination parameters on thermal lesions to biological tissue by establishing a theoretical simulation model. The study discovered that the size and form of the thermal lesion region

were significantly impacted by various frequency and duty cycle combinations. While the low-frequency and high duty cycle combination works well for deeper or larger lesions, the high-frequency and low duty cycle combination works well for precisely treating minor lesions. The findings of the simulation indicate that the smallest thermal lesion area and lowest focal temperature are produced by the combination of low frequency and low duty cycle, whereas the largest thermal lesion area and highest focal temperature are produced by the combination of high frequency and high duty cycle. These findings provide a theoretical basis for parameter selection in clinical HIFU treatment, which helps optimize treatment plans and improve treatment efficiency. Future research will use MRI-guided HIFU therapy devices and in vitro tissue tests to further examine the impact of HIFU on thermal damage to living tissue.

Acknowledgment

The anonymous reviewers' insightful remarks and recommendations are much appreciated by the authors.

Authors' Contribution

H. Dong conceived and designed the research idea and framework; G. Liu performed the simulations; and H. Dong analyzed the simulated data and wrote the manuscript. G. Peng revised the paper. All authors have read and agreed to the published version of the manuscript.

Ethical Approval

The research and usage of required resources have been approved by Changsha Normal University's School of Information Science and Engineering.

Funding

This study was funded by the Youth Fund Project of Humanities and Social Sciences Research of the Ministry of Education (22YJC-

ZH025), and the Changsha Natural Science Foundation Project (grant No.kq2202313).

Conflict of Interest

None

References

1. Biasiori-Poulanges L, Lukić B, Supponen O. Cavitation cloud formation and surface damage of a model stone in a high-intensity focused ultrasound field. *Ultrason Sonochem.* 2024;**102**:106738. doi: 10.1016/j.ultsonch.2023.106738. PubMed PMID: 38150955. PubMed PMCID: PMC10765487.
2. Moghimnezhad M, Shahidian A, Andayesh M. Multiphysics Analysis of Ultrasonic Shock Wave Lithotripsy and Side Effects on Surrounding Tissues. *J Biomed Phys Eng.* 2021;**11**(6):701-12. doi: 10.31661/jbpe.v0i0.1182. PubMed PMID: 34904067. PubMed PMCID: PMC8649164.
3. Chen Y, Lin S, Xie X, Yi J, Liu X, Guo SW. Systematic review and meta-analysis of reproductive outcomes after high-intensity focused ultrasound (HIFU) treatment of adenomyosis. *Best Practice & Research Clinical Obstetrics & Gynaecology.* 2024;**92**:102433. doi: 10.1016/j.bpobgyn.2023.102433.
4. Kung Y, Lan C, Hsiao MY, Sun MK, Hsu YH, Huang AP, et al. Focused shockwave induced blood-brain barrier opening and transfection. *Sci Rep.* 2018;**8**(1):2218. doi: 10.1038/s41598-018-20672-y. PubMed PMID: 29396523. PubMed PMCID: PMC5797245.
5. Snipstad S, Vikedal K, Maardalen M, Kurbatskaya A, Sulheim E, Davies CL. Ultrasound and microbubbles to beat barriers in tumors: Improving delivery of nanomedicine. *Adv Drug Deliv Rev.* 2021;**177**:113847. doi: 10.1016/j.addr.2021.113847. PubMed PMID: 34182018.
6. Tian H, Zhang T, Qin S, Huang Z, Zhou L, Shi J, et al. Enhancing the therapeutic efficacy of nanoparticles for cancer treatment using versatile targeted strategies. *J Hematol Oncol.* 2022;**15**(1):132. doi: 10.1186/s13045-022-01320-5. PubMed PMID: 36096856. PubMed PMCID: PMC9469622.
7. Zhu Q, Liu C, Liu L, Li Y. Effect of pulse parameters on ablation efficiency in dual-frequency HIFU therapy. *Ultrasonics.* 2023;**134**:107064. doi: 10.1016/j.ultras.2023.107064. PubMed PMID: 37331052.
8. Duclos S, Golin A, Fox A, Chaudhary N, Camelo-Piragua S, Pandey A, Xu Z. Transcranial histotripsy parameter study in primary and metastatic murine brain tumor models. *Int J Hyperthermia.* 2023;**40**(1):2237218. doi: 10.1080/02656736.2023.2237218. PubMed PMID: 37495214. PubMed PMCID: PMC10410615.
9. Quadri SA, Waqas M, Khan I, Khan MA, Suriya SS, Farooqui M, Fiani B. High-intensity focused ultrasound: past, present, and future in neurosurgery. *Neurosurg Focus.* 2018;**44**(2):E16. doi: 10.3171/2017.11.FOCUS17610. PubMed PMID: 29385923.
10. Bouakaz A, Bouhmila F, Georgiev SG, Kheloufi A, Khoufache S. Existence of classical solutions for a class of the Khokhlov–Zabolotskaya–Kuznetsov type equations. *Vladikavkaz Math J.* 2023;**25**(3):36-50. doi: 10.46698/n8469-5074-4131-b.
11. Kagami S, Kanagawa T. Weakly nonlinear propagation of focused ultrasound in bubbly liquids with a thermal effect: Derivation of two cases of Khokhlov–Zabolotskaya–Kuznetsov equations. *Ultrason Sonochem.* 2022;**88**:105911. doi: 10.1016/j.ultsonch.2022.105911. PubMed PMID: 35810619. PubMed PMCID: PMC9696949.
12. Guo GP, Li XF, Chen ZH, Meng TH, Li YZ, Ma QY. Nonlinear fields of focused acoustic-vortex beams. *Applied Acoustics.* 2024;**221**:110022. doi: 10.1016/j.apacoust.2024.110022.
13. Hasani MH, Gharibzadeh S, Farjami Y, Tavakkoli J. Unmitigated numerical solution to the diffraction term in the parabolic nonlinear ultrasound wave equation. *J Acoust Soc Am.* 2013;**134**(3):1775-90. doi: 10.1121/1.4774278. PubMed PMID: 23967912.
14. Yang X, Cleveland RO. Time domain simulation of nonlinear acoustic beams generated by rectangular pistons with application to harmonic imaging. *J Acoust Soc Am.* 2005;**117**(1):113-23. doi: 10.1121/1.1828671. PubMed PMID: 15704404.
15. Sheng R, Zhang J. Ultrasonic nonlinear fields generated from transmitters with varied aperture angles. *Applied Acoustics.* 2022;**195**:108867. doi: 10.1016/j.apacoust.2022.108867.
16. Zhou H, Huang SH, Li W. Parametric Acoustic Array and Its Application in Underwater Acoustic Engineering. *Sensors (Basel).* 2020;**20**(7):2148. doi: 10.3390/s20072148. PubMed PMID: 32290194. PubMed PMCID: PMC7180615.
17. Haddadi S, Ahmadian MT. Numerical and Experimental Evaluation of High-Intensity Focused Ultrasound-Induced Lesions in Liver Tissue Ex Vivo. *J Ultrasound Med.* 2018;**37**(6):1481-91. doi: 10.1002/jum.14491. PubMed PMID: 29193279.
18. Hajihassani M, Farjami Y, Gharibzadeh S, Tavakkoli J. A novel numerical solution to the diffraction term in the KZK nonlinear wave equation. In 38th Annual Symposium of the Ultrasonic Industry Association (UIA); IEEE; 2009. p. 1-9.
19. Davis TA, Rajamanickam S, Sid-Lakhdar WM. A survey of direct methods for sparse linear systems. *Acta Numerica.* 2016;**25**:383-566. doi: 10.1017/S0962492916000076.
20. Yuldashev PV, Karzova MM, Kreider W, Rosnitskiy PB, Sapozhnikov OA, Khokhlova VA. "HIFU Beam:" a simulator for predicting axially symmetric nonlinear acoustic fields generated by focused transducers in a layered medium. *IEEE Trans Ultrason Ferroelectr*

- Freq Control*. 2021;**68**(9):2837-52. doi: 10.1109/TUFFC.2021.3074611.
21. Irfan M, Shah FA, Nisar KS. Fibonacci wavelet method for solving Pennes bioheat transfer equation. *International Journal of Wavelets, Multiresolution and Information Processing*. 2021;**19**(06):2150023. doi: 10.1142/S0219691321500235.
 22. El-Sapa S, El-Bary AA, Albalawi W, Atef HM. Modelling Pennes', bioheat transfer equation in thermoelasticity with one relaxation time. *Journal of Electromagnetic Waves and Applications*. 2024;**38**(1):105-21. doi: 10.1080/09205071.2023.2272612.
 23. Dehbani M, Rahimi M, Rahimi Z. A review on convective heat transfer enhancement using ultrasound. *Applied Thermal Engineering*. 2022;**208**:118273. doi: 10.1016/j.applthermaleng.2022.118273.
 24. Dong H, Liu G, Tong X. Influence of temperature-dependent acoustic and thermal parameters and nonlinear harmonics on the prediction of thermal lesion under HIFU ablation. *Math Biosci Eng*. 2021;**18**(2):1340-51. doi: 10.3934/mbe.2021070. PubMed PMID: 33757188.
 25. Zou X, Qian S, Tan Q, Dong H. Formation of thermal lesions in tissue and its optimal control during HIFU scanning therapy. *Symmetry*. 2020;**12**(9):1386. doi: 10.3390/sym12091386.
 26. Gupta P, Srivastava A. Numerical analysis of thermal response of tissues subjected to high intensity focused ultrasound. *Int J Hyperthermia*. 2018;**35**(1):419-34. doi: 10.1080/02656736.2018.1506166. PubMed PMID: 30307345.
 27. Hallaj IM, Cleveland RO, Hynynen K. Simulations of the thermo-acoustic lens effect during focused ultrasound surgery. *J Acoust Soc Am*. 2001;**109**(5 Pt 1):2245-53. doi: 10.1121/1.1360239. PubMed PMID: 11386575.
 28. Heikkilä J, Curiel L, Hynynen K. Local harmonic motion monitoring of focused ultrasound surgery--a simulation model. *IEEE Trans Biomed Eng*. 2010;**57**(1):185-93. doi: 10.1109/TBME.2009.2033465. PubMed PMID: 19822463.
 29. Almekkaway MK, Shehata IA, Ebbini ES. Anatomical-based model for simulation of HIFU-induced lesions in atherosclerotic plaques. *Int J Hyperthermia*. 2015;**31**(4):433-42. doi: 10.3109/02656736.2015.1018966. PubMed PMID: 25875223.
 30. Kyriakou Z, Corral-Baques MI, Amat A, Cousios CC. HIFU-induced cavitation and heating in ex vivo porcine subcutaneous fat. *Ultrasound Med Biol*. 2011;**37**(4):568-79. doi: 10.1016/j.ultrasmedbio.2011.01.001. PubMed PMID: 21371810.
 31. Ginter S. Numerical simulation of ultrasound-thermotherapy combining nonlinear wave propagation with broadband soft-tissue absorption. *Ultrasonics*. 2000;**37**(10):693-6. doi: 10.1016/S0041-624x(00)00012-3. PubMed PMID: 10950353.
 32. Suomi V, Treeby B, Jaros J, Makela P, Anttinen M, Saunavaara J, et al. Transurethral ultrasound therapy of the prostate in the presence of calcifications: A simulation study. *Med Phys*. 2018;**45**(11):4793-805. doi: 10.1002/mp.13183. PubMed PMID: 30216469.
 33. Dong H, Liu G, Ma Zh, Peng G, Pan P. Simulation Study on the Effect of High-Intensity Focused Ultrasound on Thermal Lesion of Biological Tissue under Different Treatment Modes. *Iran J Med Phys* 2022;**19**:199-206. 10.22038/IJMP.2022.59497.1999.
 34. Sharma U, Chang EW, Yun SH. Long-wavelength optical coherence tomography at 1.7 microm for enhanced imaging depth. *Opt Express*. 2008;**16**(24):19712-23. doi: 10.1364/oe.16.019712. PubMed PMID: 19030057. PubMed PMCID: PMC2773451.
 35. Chen C, Sun A, Ju BF, Wang C. Width and depth gauging of rectangular subsurface defects based on all-optical laser-ultrasonic technology. *Applied Acoustics*. 2022;**191**:108684. doi: 10.1016/j.apacoust.2022.108684.
 36. Mei L, Zhang Z. Advances in Biological Application of and Research on Low-Frequency Ultrasound. *Ultrasound Med Biol*. 2021;**47**(10):2839-52. doi: 10.1016/j.ultrasmedbio.2021.06.005. PubMed PMID: 34304908.
 37. Jiang L, Lu G, Yang Y, Xu Y, Qi F, Li J, et al. Multichannel Piezo-Ultrasound Implant with Hybrid Waterborne Acoustic Metastructure for Selective Wireless Energy Transfer at Megahertz Frequencies. *Adv Mater*. 2021;**33**(44):e2104251. doi: 10.1002/adma.202104251. PubMed PMID: 34480501.
 38. Juang EK, De Koninck LH, Vuong KS, Gnanaskandan A, Hsiao CT, Averkiou MA. Controlled Hyperthermia With High-Intensity Focused Ultrasound and Ultrasound Contrast Agent Microbubbles in Porcine Liver. *Ultrasound Med Biol*. 2023;**49**(8):1852-60. doi: 10.1016/j.ultrasmedbio.2023.04.015. PubMed PMID: 37246049. PubMed PMCID: PMC10330369.
 39. Quarato CMI, Lacedonia D, Salvemini M, Tuccari G, Mastrodonato G, Villani R, et al. A Review on Biological Effects of Ultrasounds: Key Messages for Clinicians. *Diagnostics (Basel)*. 2023;**13**(5):855. doi: 10.3390/diagnostics13050855. PubMed PMID: 36899998. PubMed PMCID: PMC10001275.
 40. Xu Z, Hall TL, Vlaisavljevich E, Lee FT Jr. Histotripsy: the first noninvasive, non-ionizing, non-thermal ablation technique based on ultrasound. *Int J Hyperthermia*. 2021;**38**(1):561-75. doi: 10.1080/02656736.2021.1905189. PubMed PMID: 33827375. PubMed PMCID: PMC9404673.
 41. Babenko VA, Sychev AA, Bunkin NF. Optical Breakdown on Clusters of Gas Nanobubbles in Water; Possible Applications in Laser Ophthalmology. *Appl Sci*. 2023;**13**(4):2183. doi: 10.3390/app13042183.